Journal of Molecular and Engineering Materials
(2024) 2450012 (8 pages)

DOI: 10.1142/S2251237324500126

Identification of Object Roughness Using a Flexible Capacitive 3D Force Transducer Featuring an Interlocking Microstructure

Zeqian Song, Xuanzi Luo, Guanzheng Chen, Hang Yu, Lin Cheng and Aiping Liu*
Key Laboratory of Optical Field Manipulation of Zhejiang Province
College of Science, Zhejiang Sci-Tech University
Hangzhou 310018, P. R. China
**liuaiping1979@gmail.com*

Received 23 February 2024
Accepted 4 June 2024
Published 29 August 2024

A flexible capacitive three-dimensional (3D) force transducer with four bottom electrodes is proposed. A dielectric layer with ionic effects and pyramid-like microstructures is designed to improve the sensing performance of this sensor. The arrayed sensor exhibits remarkable capabilities in capturing and decoupling 3D forces, showcasing a high sensitivity, a wide response range (0–30 kPa), rapid response time (62 ms), excellent repeatability under continuous pressure, as well as static and dynamic responses. By assembling a robotic arm to grasp various objects, the sensor demonstrates exceptional sensing capabilities for object roughness, thereby highlighting its potential application as a touch recognition system in human–computer interaction scenarios.

Keywords: Sensors; capacitance; three-dimensional force; roughness.

With the advancement of mobile Internet and smart terminals, wearable electronic devices exhibit significant market potential.[1,2] As a fundamental component, flexible sensors are widely used in diverse human–computer interaction scenarios such as strain sensing, health monitoring, tactile recognition, and material identification due to their portability and exceptional wearability. Flexible sensors can be classified into various categories based on specific application contexts.[3,4] Flexible capacitive sensors with high sensitivity, good dynamic response, and mechanical stability have been widely investigated with adjustable capacitance signals by changing the effective area between the plates, the distance between the plates, and the dielectric constant of dielectric layers.[5–8] For example, a capacitive pressure sensor with interlocking microstructures formed between the electrode layer and dielectric layer was designed by Wang *et al.*[9] Through the distance adjustance between the plates via interlocking microstructure change, the sensor performance could be improved. Shi Luo *et al.* proposed a capacitive sensor with a piezoelectric ZnO film as the dielectric layer, and a polarized electric field was created when the force was applied to the ZnO film, which greatly increased the specific capacitance.[10] Hua *et al.* explored a microstructured dielectric layer to improve the compressibility and effective dielectric constant of the capacitive sensors so that the sensor capacitance

*Corresponding author.

could be changed greatly.[11] In order to adapt to more complex multi-directional force situations, a capacitance-based high-sensitivity three-dimensional (3D) force tactile sensor was designed by Wang *et al.* for grasping recognition and human motion detection.[12] Although the proposed 3D force sensor could provide spatial information of 3D force, it is still necessary and challenging to simplify the decoupling process of 3D force and improve the decoupling accuracy through ingenious structural design.

Herein, we propose an ion thin film with microstructures as the dielectric layer for constructing an array-type capacitive 3D force sensor. This approach enables accurate identification of 3D forces while concurrently enhancing the sensing performance through the incorporation of interlocking microstructures (Fig. 1). The sensitivity of the sensor can be significantly enhanced through the microstructure design of the electrode and dielectric layers, while the overall array structure design further enables accurate identification of object roughness by effectively decoupling 3D forces received by the sensor. This highlights the exceptional sensing sensitivity and recognition capability of the sensor.

Figure 1 shows the fabrication scheme of the flexible capacitive sensor, which consists of a gold upper electrode (gold-plated pyramid-like microstructure), a 2×2 array of copper lower electrode, and a dielectric layer in the middle. First, the mixture of Polyvinylidene fluoride-hexafluoropropylene (PVDF-HFP) and 1-Buty1-3-methylimidazolium Bromide ([BMIM]Br) in a given ratio was dissolved into N,N-Dimethylformamide (DMF), and then 1% Hexamethyleneimine (HMDA) as a crosslinker was added into the reaction system, and heated and stirred at 60°C for 8 h to obtain the ionic salt solution (Fig. 1(a)). Then the ionic salt solution was poured on the pyramid-shaped mold, and the mold was dried in an oven at 75°C to obtain the dielectric layer after molding (Fig. 1(b)). The copper tape attached to the Polyimide (PI) substrate was laser-cut to obtain the required lower electrode area (Fig. 1(c)). After a gold thin firm (about 3 nm in thickness) was magnetron-sputtered on another dielectric layer with microstructure, the upper electrode was obtained. The three layers were assembled with PI tape to form the sensor with interlocking microstructure (Fig. 1(d)), and the copper wires were fixed at the upper and lower electrode plates by conductive silver paste.

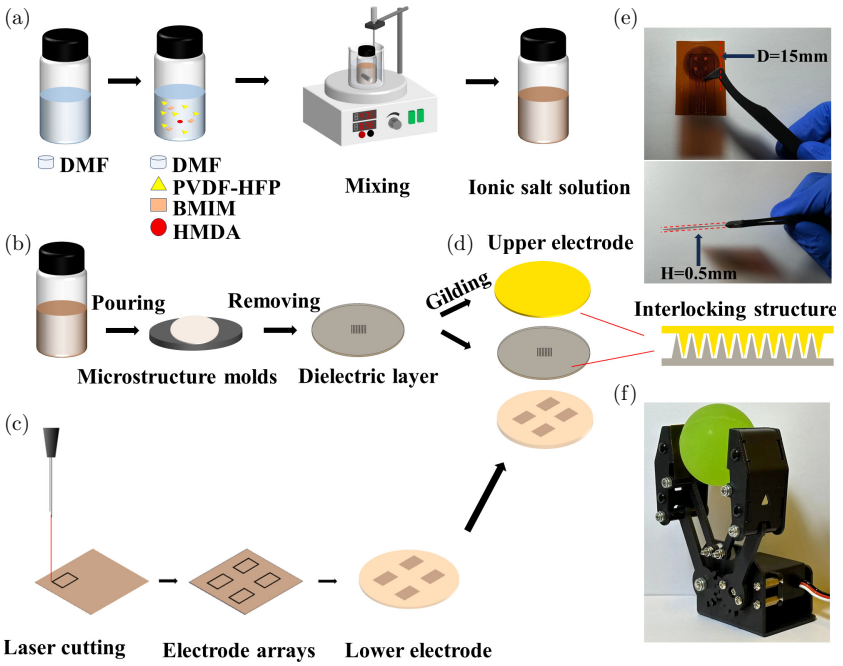

Fig. 1. Preparation process of a flexible capacitive 3D force sensor. (a) Preparation of PVDF-HFP ionic salt solution, (b) dielectric layer, and (c) lower electrode array by laser-cut copper foil. (d) The assembly of the sensor with gold-plated upper plate, dielectric layer and lower electrode to form an interlocking structure. (e) The encapsulated sensor has a 15-mm diameter and 0.5-mm thickness. (f) The sensors are mounted on the robotic arms.

The capacitive sensor has a diameter of 15 mm and a thickness of 1 mm (Fig. 1(e)), which is convenient to fix on the robotic arm for object recognition (Fig. 1(f)).

Figures 2(a) and 2(b) demonstrate the scanning electron microscopy images of the pyramid structure of dielectric and electrode layers before and after gold plating. The side length and height of the pyramid are about 40 μm and 80 μm, respectively. The spacing between pyramids is 50 μm. Ionic salt solutions are a mixture of [BMIM]Br, HMDA, and PVDF-HFP. The polymer is achieved by using HMDA as a crosslinker, cleaving N–H in HMDA, and forming C=N with C in PVDF-HFP[13] (Fig. 2(c)). For the sensing performance test, we used a digital bridge (LCR) at 100 kHz and 2 V to collect the sensor capacitance. After the sensor was placed on a mechanical test platform and a normal pressure of 0–5 kPa was applied, capacitance change with pressure was obtained (Fig. 2(d)). When changing the BMIM mass fraction in the ionic salt solution from 0% to 50%, the sensitivity of the capacitive sensor increases as the ion salt concentration increases, while its mechanical properties (estimated from the stress-strain curves, Fig. 2(e)) decrease accordingly. Tough high ion salt concentration is usually helpful in increasing sensor sensing performances, it affects the strain capacity of

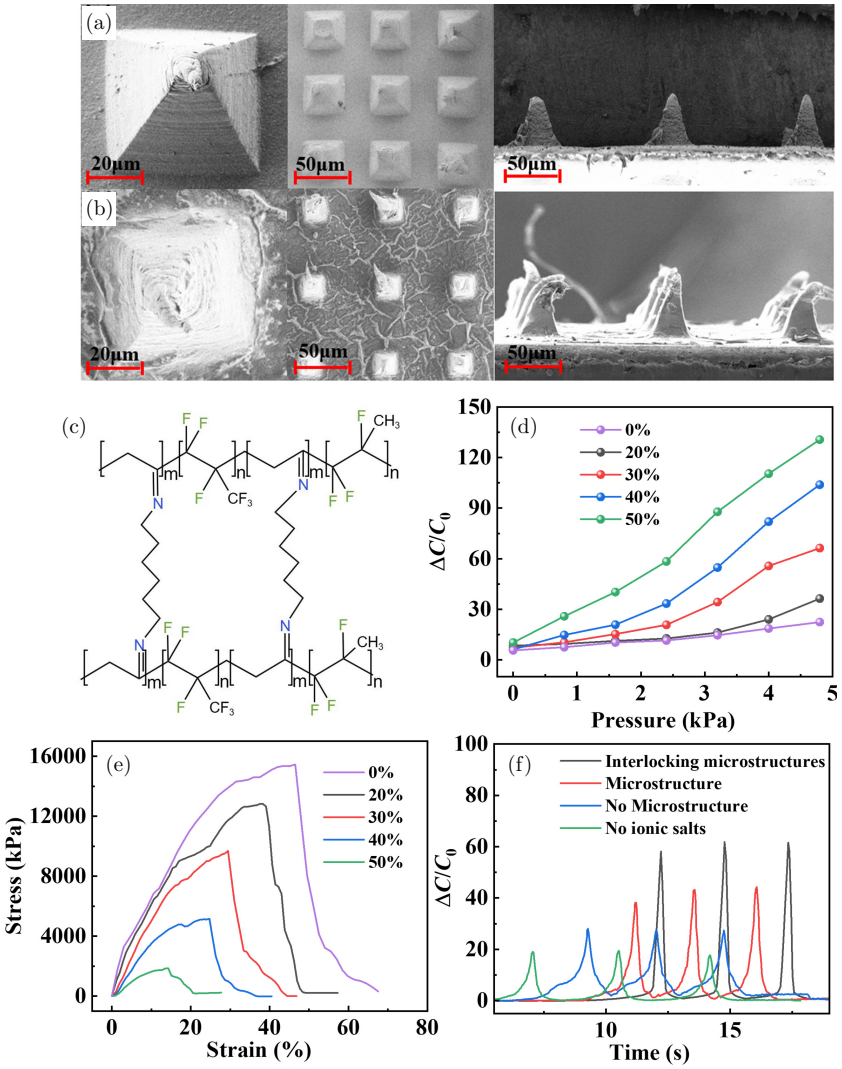

Fig. 2. (a) Surface and cross-sectional topography of the dielectric layer. (b) Surface and cross-sectional morphology of gold electrodes. (c) Structural formula of the ionic salt solution after cross-linking. (d) Effect of ionic salt concentrations on sensor performance. (e) Effect of different ionic salt concentrations on mechanical properties of the sensor. (f) The influence of microstructures and interlocking structures on sensor performance.

dielectric layer, leading to mechanical property loss. In order to ensure that the good mechanical properties were not lost and the sensing performance could be obtained at the same time, we finally selected the 30% ion salt concentration and further investigated the effect of the microstructure of the dielectric layer and interlocking structure of the sensor on the sensing capability. Figure 2(f) illustrates the sensing performance difference between different sensors with microstructure, non-microstructure, and interlocking microstructures. At 5 kPa normal pressure, the sensor with a microstructured dielectric layer displays more larger relative capacitance change ($\Delta C/C_0 = (C - C_0)/C_0$) when compared to the planar dielectric layer without microstructure in terms of the greater deformation ability of pyramid-shaped microstructure under pressure.[14] The addition of [BMIM]Br with ionic effects can further improve the force-sensitive effect of the sensor because a polarized electric field will be created in the ionic film under a force, which greatly increases the specific capacitance.[15] When the sensor with interlocking structure is compressed by external force, the capacitance increase is not only caused by the enormous decrease in the electrode gap but also by the increase of the effective permittivity of the dielectric layer.[9] The sensor also exhibits excellent signal reproducibility during multiple pressurization and unloading processes (Fig. 2(f)).

Figure 3(a) shows the $\Delta C/C_0$ of the sensing unit in the sensor when applying a normal force of 0–30 kPa to the top electrode of the sensor. The sensitivity S ($S = (\Delta C/C_0)/\Delta P$), where P is the average force of the sensor per unit area) presents a three-stage change. In the pressure range of 0–10 kPa, $S = 1.84\,\text{kPa}^{-1}$ is lower due to the incomplete deformation of the microstructure between the dielectric layer and electrode layer of the sensor, and the gap in the interlocking structure is not sufficiently reduced.[11] With the increase of pressure to 10–15 kPa, the microstructure is completely deformed, and the gap in the interlocking structure is also fully reduced, raising sensor sensitivity up to $10.47\,\text{kPa}^{-1}$.

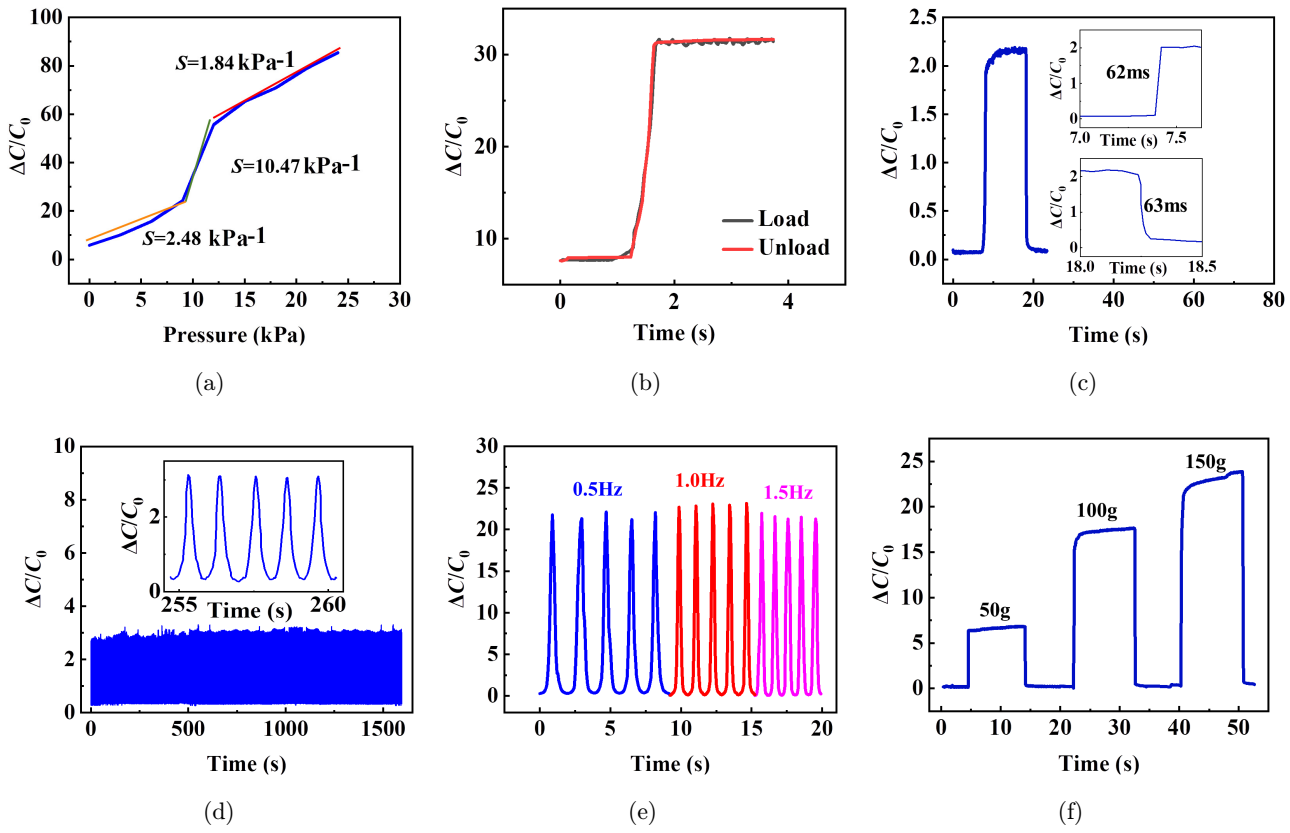

Fig. 3. Sensing properties of flexible capacitive 3D force transducers. (a) The sensor sensitivity in the range of 0–30 kPa. (b) The sensor has good hysteresis. (c) Sensor stability at 2 kPa positive pressure during 2000 tests. (d) Response time at 2 kPa normal force. (e) Dynamic response at different frequencies. (f) Static response at different pressures.

When further increasing the pressure to 15–30 kPa, S decreases to 2.48 kPa^{-1} due to the gradually saturated deformation in dielectric layer and electrode layer. The hysteresis of the sensor was measured during loading and unloading processes in the positive pressure range of 0–30 kPa. The sensor has good hysteresis and robustness (Fig. 3(b)), and shows a stable sensing signal during 2000 repeated loading-unloading cycles (Fig. 3(c)) under 2 kPa. The response time at 2 kPa is about 60 ms at a loading and unloading speed of 50 mm/min (Fig. 3(d)), which indicates its good response ability under the action of normal force. The $\Delta C/C_0$ of the sensor at different loading frequencies (0.5 Hz, 1.0 Hz and 1.5 Hz) under 20 kPa is independent of the frequency (Fig. 3(e)), and the capacitive response to different static pressures of 50 g, 100 g and 150 g is very stable (Fig. 3(f)).

For the detection and recognition of a 3D force in space, Figs. 4(a)–4(c) show the $\Delta C/C_0$ with a 0–5 N force applied to the sensor in the X-axis, Y-axis, and Z-axis, respectively. When we give the sensor a force along the X-axis, the overlap areas of Capacitors C2 and C3 increase, while the ones of Capacitors C1 and C4 decrease, leading to a positive capacitance increment for C2 and C3 and a negative one for C1 and C4 (Fig. 4(a)). The same is true of this rule for the situation along Y-axis forces (Fig. 4(b)). When the sensor is applied a force along the Z-axis, the spacing between upper and lower plates obviously decreases, resulting in positive capacitance increment for Capacitors C1, C2, C3, and C4 (Fig. 4(c)). This one-to-many structure of the upper and lower plates cleverly decomposes the capacitance change on the change of overlapping area A between the plates and the change of the distance d between the plates, so as to quantify the magnitude and direction of the 3D force. The capacitance of this sensor can be given by the following formula:

$$C = \varepsilon_r \varepsilon_0 \frac{A + \Delta A}{d + \Delta d}. \tag{1}$$

Here ε_r is the dielectric constant of the dielectric layer (about $\varepsilon_r \approx 8.3 \times 10^{-12}$F/m)[16] and ε_0 is the dielectric constant of the air ($\varepsilon_0 = 1.0 \times 10^{-12}$F/m),

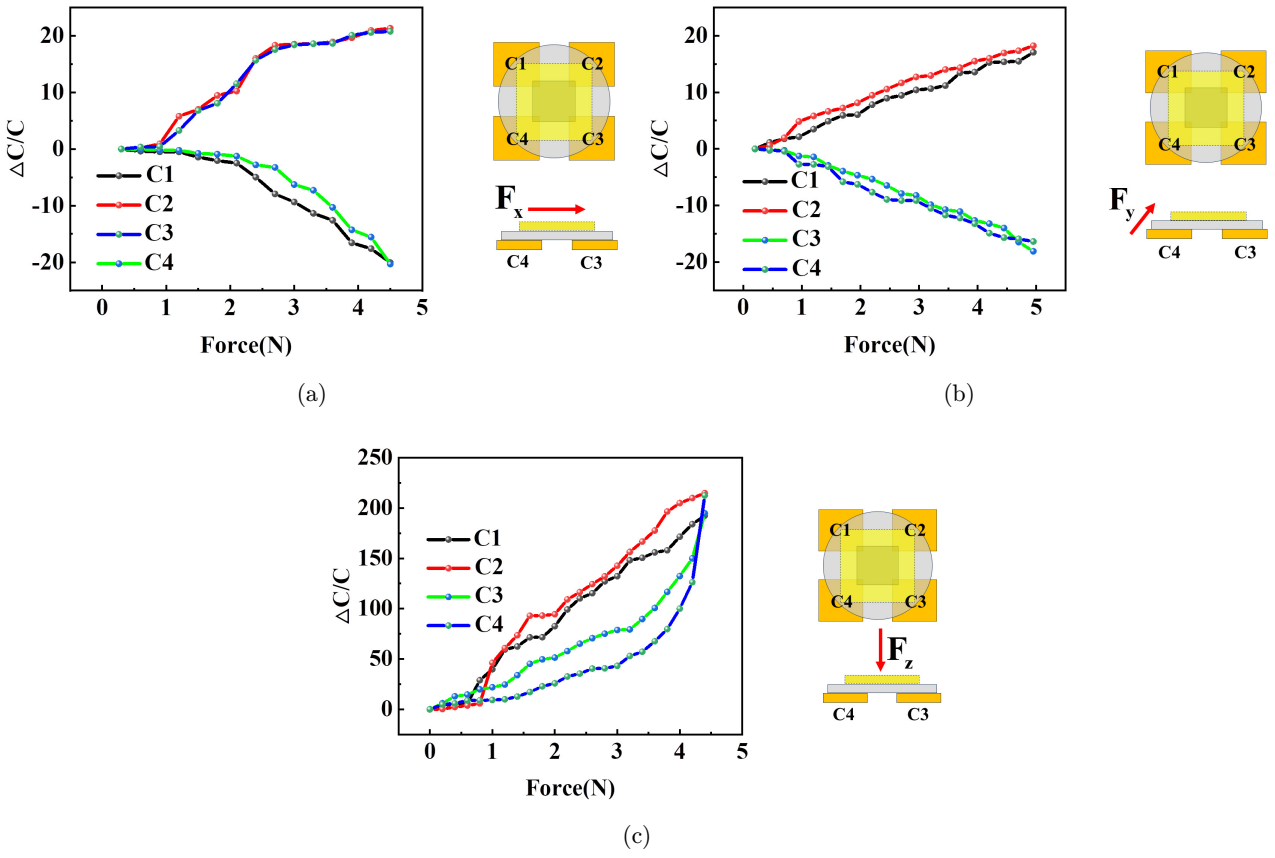

Fig. 4. Calibration and verification of 3D forces. (a) An X-axial force, (b) a Y-axial force and (c) a Z-axial force is applied to the sensor.

ΔA is the overlapping area change of upper and lower plates under stress, and Δd is the spacing change of upper and lower plates under stress. Through Eq. (1), we can decouple capacitance change into the changes of S and d caused by the 3D force. We can further simplify Eq. (1) by using $\Delta C = \varepsilon(\Delta A/\Delta d)$ $(\varepsilon = \varepsilon_r \varepsilon_0)$,

$$\Delta C = C - C_0 = \varepsilon \frac{\Delta A}{\Delta d}. \tag{2}$$

To further verify the accuracy of this decoupling method, we applied a linear force of 0–5 N to the sensor on 30°, 45°, and 60° inclined tables, respectively (Figs. 5(a)–5(c)). Under the action of vertical downward force, with the slope increase of the inclined platform, the normal force of the sensor decreases, and the tangential force increases. Since the $\Delta C/C_0$ under the action of the normal force is much greater than the $\Delta C/C_0$ under the action of the tangential force (Figs. 4(a)–4(c)), with the slope increase of the inclined platform, the $\Delta C/C_0$ also decreases. This proves that the decoupling method is suitable for the sensor,[17] and can make a good distinction for stresses with different magnitudes and directions. The above decoupling analysis indicates that the proposed sensor has the function of decoupling 3D forces.

We further explore the sensor application in the recognition of material roughness. The sensor is fixed on the robotic arm (Fig. 1(f)), and the different materials fixed on the operating table are clamped by the robotic arm with a 5N force. The roughness information is judged by capturing the waveform change and peak value of each capacitance of the capacitance array.[18] As shown in Figs. 6(a)–6(c), when the clamping force F_N (constant force) of the mechanical arm is programmed to control, the dynamic friction force (F_s) of the sensor attached to the mechanical arm is directly proportional to the friction coefficient (f_s) of the material.[19] The sandpaper with 240Cw has the largest f_s, and therefore demonstrates the largest F_s under a certain F_N. This indicates that the sensor can distinguish the object's roughness. In addition, a time-delay grasping test was carried out on the nonwoven fabric, A4 white paper, and copper foil via the mechanical arm that assembled the sensor (Figs. 6(d)–6(f)). The different crests and waveforms in the

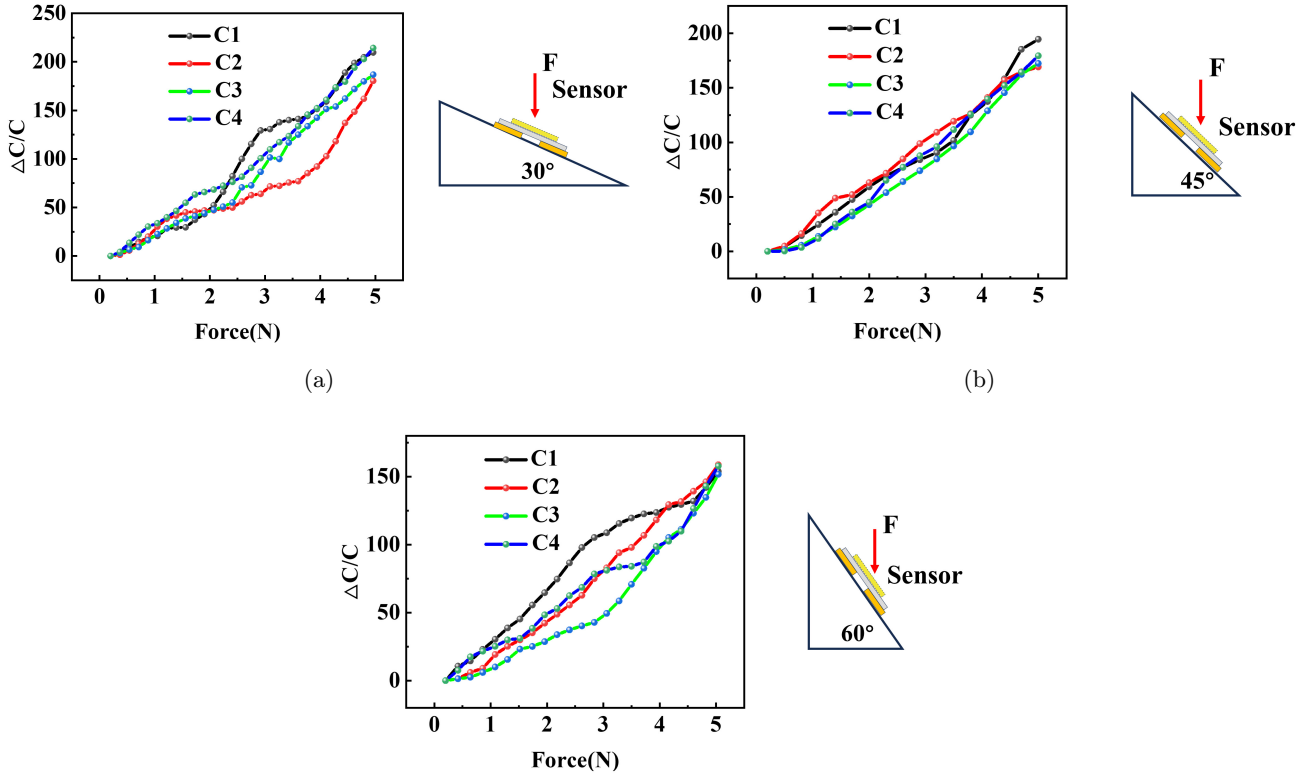

Fig. 5. A Z-axial force is applied to the sensor placed on a (a) 30°, (b) 45° and (c) 60° inclined stages.

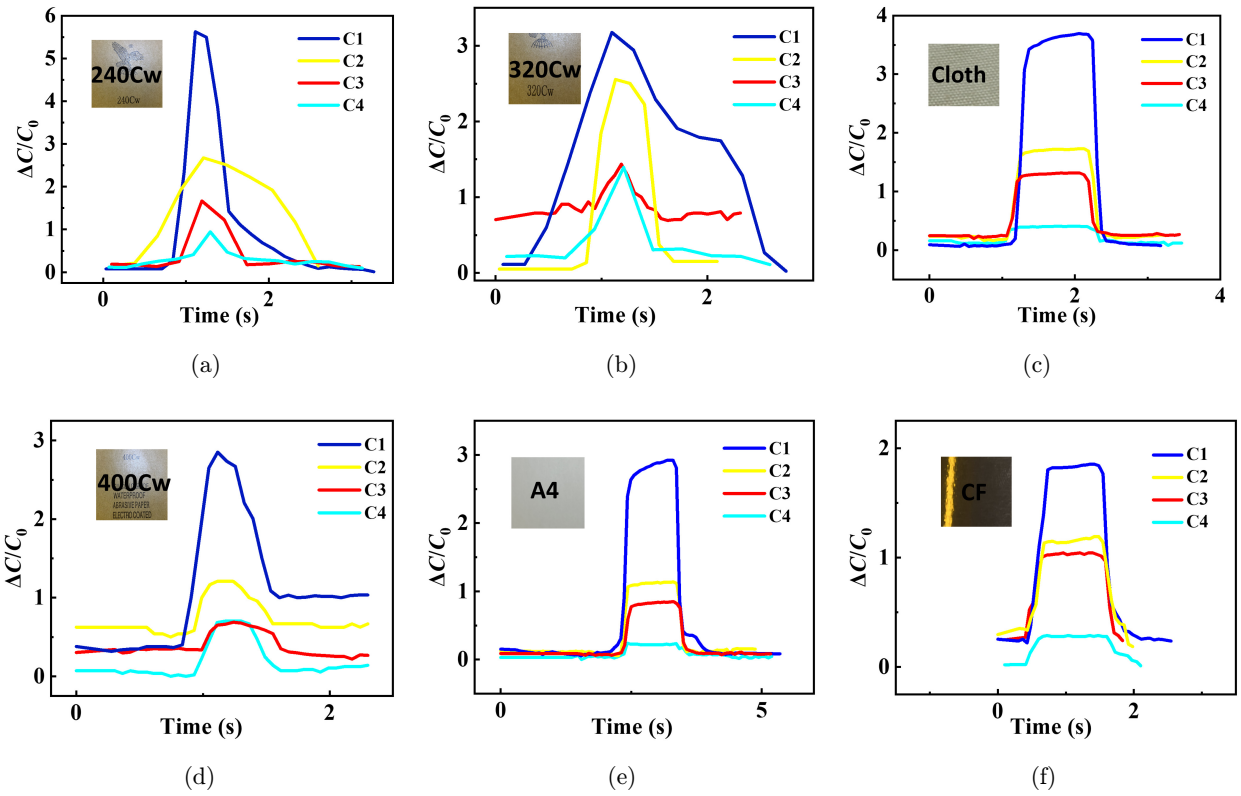

Fig. 6. Flexible capacitive 3D force transducers are used to distinguish different materials and roughness. Capacitance change when gripping (a) 240Cw, (b) 320Cw and (c) 400Cw sandpaper. Capacitance change when gripping (d) nonwoven fabric, (e) A4 paper and (f) copper foil.

diagram reflect different materials and different roughnesses, with coarse fabrics having higher crests and smooth copper foil having the lowest crests. This demonstrates that the sensor can help the robotic arm perceive external information and even quantify the roughness of an object beyond the human hand.[20]

In conclusion, we designed a flexible capacitive 3D force sensor with an interlocking structure between the upper electrode and dielectric layer, and the arrayed sensor can easily decouple the 3D force by the change of overlapping area and the distance between the plates.[21] The designed sensor also shows good sensing performance and practicability in actual material roughness recognition, showing its great potential in the human–computer interaction and material recognition.

Acknowledgments

This work was supported by the National Natural Science Foundation of China (12272351, 12372168 and 11972323), the Zhejiang Provincial Natural Science Foundation of China Z24A020008 and LR20A020002), the "Pioneer" and "Leading Goose" R&D Program of Zhejiang (2023C01051).

ORCID

Aiping Liu https://orcid.org/0000-0002-2338-062X

References

1. X. F. Wang *et al.*, *Sens. Actuators A, Phys.* **330**, 112838 (2021).
2. L. Cheng *et al.*, *J. Mater. Chem. C* **11**, 8413 (2023).
3. H. R. Lim *et al.*, *Adv. Mater.* **32**, 1901924 (2021).
4. L. Wei *et al.*, *Sens. Actuators B, Chem.* **379**, 133213 (2023).
5. R. B. Mishra *et al.*, *Adv. Mater. Technol.* **6**, 2001023 (2021).
6. S. P. Ji *et al.*, *Funct. Mater. Lett.* **16**, 2350010 (2023).
7. H. Z. Wang *et al.*, *J. Mater. Chem. C* **10**, 1594 (2022).

8. Z. H. Lv *et al.*, *Funct. Mater. Lett.* **15**, 2250026 (2022).
9. S. Wang *et al.*, *IEEE Trans. Euros.* **33**, 8808583 (2019).
10. S. Luo *et al.*, *Nano Energy* **80**, 105580 (2021).
11. T. Hua *et al.*, *Sensors* **23**, 4323 (2023).
12. Y. F. Wang *et al.*, *Smart Mater. Struct.* **31**, 095013 (2022).
13. G. H. Chen *et al.*, *Adv. Energy Mater.* **8**, 1801219 (2018).
14. S. R. A. Ruth *et al.*, *Adv. Funct. Mater.* **30**, 1903100 (2020).
15. I.-T. Kim *et al.*, *Electrochimica Acta.* **55**, 6632 (2010).
16. Z. Ding *et al.*, *Nano Res.* **16**, 9443 (2023).
17. T. P. Xu *et al.*, *Measurement.* **202**, 111876 (2022).
18. Q. Zhou *et al.*, *J. Mater. Chem. A* **7**, 27334 (2019).
19. S. Kim *et al.*, *Soft Robot.* **9**, 119 (2022).
20. M. Ha *et al.*, *Adv. Funct. Mater.* **25**, 2841 (2015).
21. Q. Hua *et al.*, *Nat. Commun.* **9**, 244 (2018).